

Direct Insertion of MODIS Radiances in a Global Aerosol Transport Model

CLARK WEAVER,* ARLINDO DA SILVA,⁺ MIAN CHIN,[#] PAUL GINOUX,[@] OLEG DUBOVIK,^{&,@@}
DAVE FLITTNER,** AAHMAD ZIA,[#] LORRAINE REMER,⁺⁺ BRENT HOLBEN,[&] AND WATSON GREGG^{##}

*Goddard Earth Sciences and Technology Center, University of Maryland, Baltimore County, Baltimore, Maryland

+ Global Modeling and Assimilation Office, NASA Goddard Space Flight Center, Greenbelt, Maryland

Atmospheric Chemistry and Dynamics Branch, NASA GSFC, Greenbelt, Maryland

@ NOAA/Geophysical Fluid Dynamics Laboratory, Princeton, New Jersey

& Biospheric Sciences Branch, NASA GSFC, Greenbelt, Maryland

** Climate Sciences Branch, NASA Langley Research Center, Langley, Virginia

++ Climate and Radiation Branch, NASA GSFC, Greenbelt, Maryland

Ice and Ocean Branch, NASA GSFC, Greenbelt, Maryland

(Manuscript received 24 June 2005, in final form 15 February 2006)

ABSTRACT

In this paper results are presented from a simple offline assimilation system that uses radiances from the Moderate Resolution Imaging Spectroradiometer (MODIS) channels that sense atmospheric aerosols over land and ocean. The MODIS information is directly inserted into the Goddard Chemistry and Aerosol Radiation Transport model (GOCART), which simulates the following five aerosol types: dust, sea salt, black carbon, organic carbon, and sulfate. The goal is to produce three-dimensional fields of these aerosol types for radiative forcing calculations.

Products from this assimilation system are compared with ground-based measurements of aerosol optical depth (AOD) from the Aerosol Robotic Network (AERONET). Insertion of MODIS radiances draws the GOCART model closer to the AERONET AOD. However, there are still uncertainties with surface reflectivity over moderately bright surfaces and with the amount of absorbing aerosol.

Also described is the assimilation cycle. The forward model takes the aerosol information from the GOCART model and calculates radiances based on optical parameters of the aerosol type, satellite viewing angle, and the particle growth from relative humidity. Because the GOCART model is driven by previously assimilated meteorology, these forward model radiances can be directly compared with the observed MODIS level-2 radiances. The offline assimilation system simply adjusts the aerosol loading in the GOCART model so that the observed minus forward model radiances agree. Minimal change is made to the GOCART aerosol vertical distribution, size distribution, and the ratio of the five different aerosol types. The loading in the GOCART model is updated with new MODIS observations every 6 h. Since the previously assimilated meteorology provides surface wind speed, radiance sensitivity to wind speed over rough ocean is taken into account. Over land the dark target approach, also used by the MODIS-atmosphere group retrieval, is used. If the underlying land surface is deemed dark enough, the surface reflectances at the 0.47- and 0.66- μm wavelengths are constant multiples of the observed 2.13- μm reflectance. Over ocean the assimilation AOD compares well with AERONET, over land less so. The results herein are also compared with AERONET-retrieved single-scattering albedo. This research is part of an ongoing effort at NASA Goddard to integrate aerosols into the Goddard Modeling and Assimilation Office (GMAO) products.

1. Introduction

Accurate global representations of the spatial distributions of the major tropospheric aerosols species are

^{@@} Current affiliation: Laboratoire d'Optique Atmosphérique, Université de Lille, Villeneuve d'Ascq, France.

Corresponding author address: Dr. Clark J. Weaver, NASA Goddard Space Flight Center, Code 613.3, Greenbelt, MD 20771.
E-mail: weaver@blueberry.gsfc.nasa.gov

needed for many reasons. These include, but are not limited to, the need 1) to reduce the uncertainty in aerosol forcing of climate (Ramaswamy et al. 2001), 2) to quantify aerosol radiative forcing in the thermodynamic equation of GCMs, 3) to account for the reduction of photochemical reaction rates due to presence of aerosols (Martin et al. 2003), and 4) to account for dust extinction in retrievals of temperature and humidity from IR sensors [e.g., Television Infrared Observation Satellite (TIROS) Operational Vertical Sounder (TOVS) and Atmospheric Infrared Sounder (AIRS)

radiances; Weaver et al. 2002, 2003; Nalli and Stowe 2002].

Simulated aerosol fields from current aerosol transport models and fields of aerosol products from satellite retrievals are used to meet these needs. Each has their strengths and weaknesses. While satellite retrievals strive to give accurate values of the aerosol optical depth (AOD) and sometimes size distribution information, they lack vertical information and hourly global coverage, and suffer from missing data in cloudy regions. On the other hand, global aerosol simulations have improved significantly in the last few years, but they still sometimes do not validate well against observations. This indicates that unknown physical mechanisms are missing or incorrect. For example an offshore ocean location that has low aerosols based on satellite observations may be incorrectly simulated in a model due to an overly enthusiastic nearby source location.

Weaknesses in both the simulations and retrieved products motivate the development of an aerosol assimilation system that strives to take the accurate information from both approaches and merge them into aerosol fields with high spatial and temporal resolution. Previous studies have assimilated the aerosol optical depths from satellite retrievals. Collins et al. (2001) assimilated the Advanced Very High Resolution Radiometer (AVHRR) optical depths in the Model of Atmospheric Transport and Chemistry (MATCH). Wang et al. (2004) assimilated Geostationary Operational Environmental Satellite (GOES) AOD using a mesoscale model. Rather than assimilate satellite AOD, we choose a more fundamental quantity—the observed radiances. Any satellite retrieval needs to make assumptions about the aerosol type, size, and optical properties in order to obtain AOD. However, these assumptions may be inconsistent with the aerosol transport model assimilating the retrievals. At each assimilation cycle some of the difference between the transport model-derived AOD and the retrieved AOD may simply be due to these inconsistent assumptions. Assimilating the radiances avoids this issue; moreover, it allows information from the aerosol transport model to be used to interpret the radiances.

This is the ultimate goal of the Goddard Aerosol Assimilation System (GAAS), an ongoing effort at the Laboratory for Atmospheres at National Aeronautics and Space Administration (NASA) Goddard Spaceflight Research Center to assimilate aerosols. Specifically, the goal is to incorporate aerosols into the operational assimilation system at the Global Modeling and Assimilation Office (GMAO). The major tropospheric species will be simulated online in the Finite Volume

General Circulation Model (fvGCM) and assimilated with radiances of several satellite observing systems. Aerosol diabatic heating will be included in the fvGCM thermodynamic equation and aerosol extinction will be included in the retrievals of temperature and moisture from satellite-based infrared sensors (e.g., TOVS and AIRS).

We have developed and tested the analysis module of the assimilation system offline using Moderate Resolution Imaging Spectroradiometer (MODIS) radiances and the Goddard Chemistry and Radiation Transport Model (GOCART). This paper presents preliminary results from this offline system.

2. Description of assimilation/retrieval system

Figure 1 shows a schematic of the offline assimilation system. At the top, the GOCART model provides a 6-h first guess (forecast) of the five tropospheric aerosols. The 3D fields of mass mixing ratio for the various size bins that GOCART simulates are concatenated into a state vector, \mathbf{w}^f . The “f” superscript denotes that the state vector consists of first-guess values. The forward model is a radiative transfer model that calculates the reflectances that MODIS would observe based on the input GOCART forecast, \mathbf{w}^f . Mathematically, the forward model is symbolized by the \mathbf{h} operator; its output is $\mathbf{h}\mathbf{w}^f$. The quality control computes the difference between the first-guess and the actual observed MODIS reflectances. This residual is then used by the analysis to adjust the 3D aerosol concentrations so that they agree with the observed MODIS reflectances. The “a” superscript of the resulting state vector, \mathbf{w}^a , denotes that it consists of analysis values.

If we are doing an assimilation then the adjusted 3D concentrations \mathbf{w}^a are used as an initialization by GOCART to provide another 6-h forecast (shown by the dotted arrows). Since information from a MODIS pixel is inserted only at the nearest GOCART grid point, this is termed direct insertion. In other more sophisticated assimilation systems information from a MODIS pixel will influence several surrounding grid points. We choose the more simplified approach here.

If we are doing a retrieval then the dotted lines in Fig. 1 are ignored and the analysis aerosol concentrations are not inserted into the GOCART model. Rather, the first-guess fields are from a free-running (usually previously run) GOCART model that has had no MODIS information insertion (shown by dashed arrows). The retrieved aerosol optical depth and single-scattering albedo output from the analysis module are called GOCART retrievals since the assumptions that were used in the retrieval are from the GOCART model.

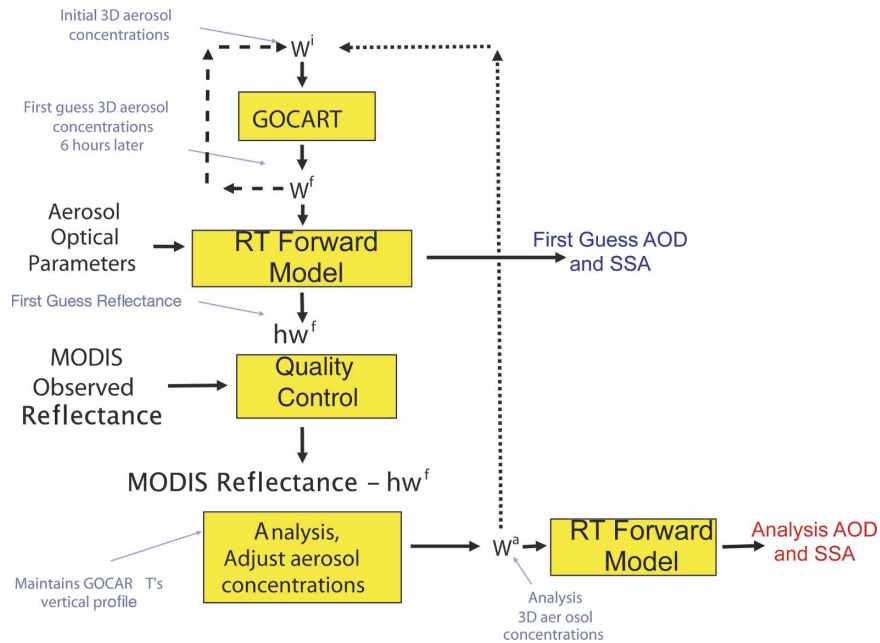


FIG. 1. Schematic diagram of the aerosol retrieval/assimilation from MODIS radiances. For the retrieval the GOCART model is first run offline without any MODIS information insertion (shown by the dashed arrow cycle). The retrieval takes the first-guess concentrations of aerosol (w^f) from the GOCART simulation and produces first-guess and analysis AOD and scattering albedo via the solid arrows. The offline assimilation uses previously calculated analysis concentrations (w^a) as an initialization for the GOCART model as shown by the dotted arrows. The dashed lines are ignored. See text.

These are different from the retrievals from the MODIS–atmosphere working group (MAG; Remer et al. 2005); they use a different set of assumptions.

a. GOCART model

The GOCART model is fully described in (Chin et al. 2002, 2004). It is an offline transport model driven by assimilated meteorological fields from the Goddard Earth Observing System Data Assimilation System, GEOS-DAS (Schubert et al. 1993). In the troposphere, the transport model grid is identical to the archived assimilation grid. Currently, the transport model horizontal resolution is 2.0° latitude \times 2.5° longitude, with 30 vertical levels. The vertical resolution depends on the assimilation system chosen and ranges from 500 m at the earth's surface and 2 km at the model top. The horizontal advection scheme is a three-dimensional flux form semi-Lagrangian scheme (Lin and Rood 1996). The model accounts for convective and diffusive transport by using archived cloud convective mass flux and vertical eddy diffusion coefficients. The model accounts for gravitational settling, removal at the surface by turbulent and molecular diffusion, and wet removal in and below clouds.

The mineral dust module is described in Ginoux et al.

(2001). It transports four size ranges from 0.1 to $10 \mu\text{m}$. The dust source module is based on archived surface wetness, terrain, local wind speed, and eddy diffusion. The module requires an estimate of the total global emission. A value of 2200 Tg yr^{-1} seems to yield results that are in good agreement with the ground-based observations.

The sulfate module simulates three species: dimethyl sulfide (DMS), SO_2 , and SO_4 . Other reactive species (e.g., NO_x , O_3 , H_2O_2) are prescribed by monthly mean climatologies. The model results have been thoroughly validated with ground-based measurements, field experiments, and sulfur model intercomparisons. The carbon module simulates four types of carbonaceous aerosol: hydrophilic, hydrophobic, black, and organic carbon. Biomass burning emissions are taken from seasonal and interannual variations in the burned biomass (Duncan et al. 2003) based on satellite observations of global fire counts and an annual mean burned biomass inventory. Anthropogenic emissions are from the global dataset of Cooke et al. (1999).

Sea-salt aerosols are simulated using the flux parameterization of Monahan et al. (1986). The transport and removal processes for the four size classes are similar for the other hygroscopic aerosols. The GOCART

TABLE 1. Coefficients for GOCART model error covariance matrix on the diagonal.

	Ocean	Land
Dust	1.00	1.00
Sea salt	1.00	1.0×10^{-4}
Black carbon	1.0×10^{-2}	5.0×10^{-3}
Pure organic carbon	1.00	1.00
Sulfate	1.00	1.00

model transports the dry mass of the hydrophilic components of: sulfate, black and organic carbon, and sea salt. The effective radius used in the radiative transfer calculations of the forward model accounts for the ambient relative humidity estimated by GEOS-DAS. The growth functions are taken from the Global Aerosol Data Set (Kopke et al. 1997) and described Chin et al. (2002).

b. Analysis

The analysis strives to produce a best estimate of the actual 3D aerosol concentrations \mathbf{w}^a based on the MODIS reflectances and the GOCART first guess. Equation (1) shows the likelihood or cost function that when minimized will yield this best estimate ($\mathbf{w} = \mathbf{w}^a$). Since this is a direct insertion assimilation, we can solve the cost function for each individual grid point only using MODIS observations and GOCART information pertaining to that point:

$$J(\mathbf{w}) = (\mathbf{w} - \mathbf{w}^f)^T (\mathbf{P}^f)^{-1} (\mathbf{w} - \mathbf{w}^f) + (\mathbf{y}^o - \mathbf{h}\mathbf{w})^T (\mathbf{R}^o)^{-1} (\mathbf{y}^o - \mathbf{h}\mathbf{w}), \quad (1)$$

where $\mathbf{w} - \mathbf{w}^f$ is the difference in aerosol concentrations: the best estimate (\mathbf{w}) minus first guess from GOCART (\mathbf{w}^f); \mathbf{P}^f is the GOCART error covariance matrix; $\mathbf{y}^o - \mathbf{h}\mathbf{w}$ is the difference in reflectances: MODIS observations (\mathbf{y}^o) minus the best estimate from the forward model ($\mathbf{h}\mathbf{w}$); and \mathbf{R}^o is the error covariance matrix of MODIS reflectances.

Even though we need to do this solution for each of the GOCART grid points that has cloud-free MODIS reflectances (1304 grid points for $2^\circ \times 2.5^\circ$ resolution), it is computationally feasible. A full 3D analysis that allows an MODIS observation to influence more than one GOCART grid point would have one solution each

time step. However, the state vector would be prohibitively large since it would include all 3D GOCART information. This approach is computationally much more expensive but will be implemented in a later version of GAAS. The final solution \mathbf{w}^a is dependent on the choice of the two error covariance matrices \mathbf{P}^f and \mathbf{R}^o .

Tables 1 and 2 show the diagonal values for the error covariance matrices used in this study. All the uncertainties in the GOCART model (the driving winds, the transport algorithm, and the aerosol source and removal terms) are lumped together in \mathbf{P}^f . All the uncertainties in the observations (e.g., the calibration and the cloud contamination) and uncertainties in the radiative transfer model (e.g., the assumed optical parameters, the reflectivity of the underlying surface, the chlorophyll concentrations) are all apart of \mathbf{R}^o . If \mathbf{P}^f is large the solution \mathbf{w} will draw away from the GOCART model but the simulated reflectances will be close to the observation. Likewise, assuming large errors on the MODIS observations (\mathbf{R}^o) will yield a solution close to the GOCART first guess ($\mathbf{w}^a = \mathbf{w}^f$).

We solve Eq. (1) iteratively using a nonlinear quasi-Newton relation:

$$\mathbf{w}_{i+1} = \mathbf{w}^f + \mathbf{P}^f \mathbf{H}_i^T (\mathbf{H}_i \mathbf{P}^f \mathbf{H}_i^T + \mathbf{R}^o)^{-1} [\mathbf{y}^o - \mathbf{h}(\mathbf{w}_i) + \mathbf{H}_i(\mathbf{w}_i - \mathbf{w}^f)], \quad (2)$$

where the Jacobean of the forecast model is $\mathbf{H}_i = \partial \mathbf{h}\mathbf{w} / \partial \mathbf{w} | \mathbf{w} = \mathbf{w}_i^f$. The i denotes the iteration number. This relation assumes that the forecast and observations are unbiased, with statistically independent errors. Except for possibly the $0.470\text{-}\mu\text{m}$ channel, there is little information about the vertical distribution of aerosols in the MODIS reflectances. To simplify the solution we only use total column masses of the GOCART species in the state vector \mathbf{w}^f :

$$\mathbf{w}^f = [\text{Dust}_1, \dots, \text{Dust}_4, \text{Salt}_1, \dots, \text{Salt}_4, \text{BC}_{\text{dry}}, \text{BC}_{\text{wet}}, \text{OC}_{\text{dry}}, \text{OC}_{\text{wet}}, \text{Sulfate}] \quad (3)$$

where Dust_j is total column mass carried by the smallest dust size bin in GOCART, Salt_j is the smallest sea-salt bin, BC_{dry} is the hydrophobic black carbon, and OC_{wet} is the hydrophilic organic carbon. These 13 ele-

TABLE 2. Coefficients for the observational MODIS error covariance matrix on the diagonal.

	0.470	0.560	0.660	0.870	1.24	1.64	2.13
Channel wavelengths	0.30	0.20	0.10	0.001	0.1	0.1	0.005
Ocean values	0.001	x	0.300	0.300	x	x	0.300
Land values							

ments are the only information from the GOCART model that is used in the solution. The forecast model error covariance is a 13×13 matrix with diagonal elements of \mathbf{w}^f times the coefficients in Table 1 and with zeros for the off-diagonal elements.

Over ocean the observable vector \mathbf{y}^o for a specific GOCART grid point consists of a seven-element vector of reflectances at wavelengths of 0.47, 0.55, 0.66, 0.87, 1.24, 1.64, and 2.13 μm . At each analysis cycle all the cloud-free MODIS level-2 reflectances within the GOCART grid box that were sampled within ± 3 h of the analysis time are averaged. These reflectances are a product of the MODIS aerosol algorithm developed by the MODIS atmosphere retrieval group. They have already been screened for clouds, inappropriate surface features, and inconsistencies. The observation error covariance \mathbf{R}^o is a 7×7 matrix with values listed in Table 2 on the diagonal elements and zeros elsewhere. The analysis trusts information with smaller error values and ignores information associated with larger error. Since aerosols in general have strong extinction at 0.87 μm , we chose a low error covariance value for this channel. Likewise the radiance at the 0.47- μm channel is given the largest error because the radiance here may be influenced by chlorophyll absorption. We should clarify that the actual radiance values at 0.47 and 0.87 μm are equally accurate, but that the 0.47 μm has less useful aerosol information. Over land there are level-2 radiances only for four channels: 0.47, 0.66, 0.87, and 2.13 μm . However, we are effectively using information from only the 0.47- μm channel. When we used information from both the 0.47 and 0.66 channels, the resulting species distributions were radically different from the GOCART model. We suspect that errors in the estimated surface reflectance are to blame.

The choice of the model error covariance is to some degree arbitrary and it involves assumptions that are difficult to justify. For example the model and observational errors are assumed to be unbiased and normally distributed.

c. Forward model

The University of Arizona Radiation Transfer Code (RTC) is the basis for the forward model (Herman and Browning 1965). It assumes a plane-parallel, cloud-free atmosphere and accounts for polarization by carrying the four Stokes parameters. Rather than running the RTC for each GOCART grid point, which would be computationally impossible, the forward model consists of two sets of lookup tables (LUT) of precomputed radiance calculations: one for rough ocean surface and

one for land surfaces. Both sets of lookup tables account for polarization and use the same assumptions about aerosol optical parameters and size distribution.

Over land each LUT consists of 1) the reflectance assuming a surface albedo of zero (ρ_0), 2) the atmospheric transmittance (T), and 3) the atmospheric backscatter (\bar{S}). These are stored as a function of satellite viewing geometry, the aerosol optical depth at 0.56 μm , and the channel wavelength. If we assume the surface is Lambertian the reflectance at nonzero surface albedo (ρ) is calculated from

$$\rho = \rho_0 + T\rho_{\text{surf}}/(1 - \bar{S}\rho_{\text{surf}}). \quad (4)$$

Uncertainty in the surface reflectance ρ_{surf} and error from the Lambertian assumption both lead to significant error in the simulated reflectance. We try to minimize this error by drawing to the MODIS radiances at locations with the darkest targets and only drawing to shortest wavelength channels (0.47 μm). Airborne spectral measurements of the bidirectional reflectance distribution function (BRDF) over several southern Africa ecosystems are reported by Gatebe et al. (2003). The site that comes closest to resembling the scenes with low surface reflectance is Skukuza (25.0°S, 31.5°E). Here the surface reflectance varies from 0.02 to 0.08 over the MODIS scan angles for the 0.472- μm channel. Based on the change of AOD with reflectance, we estimate the error from the Lambertian assumption to be on the order of 0.1 AOD.

Over ocean we can calculate the BRDF from the surface wind speed. Over ocean there are LUTs for 2, 6, and 12 m s^{-1} surface wind speeds. In sum we account for four different surface conditions: one Lambertian over land and three surface wind conditions over ocean. There is further discussion on the surface reflectances in the next section.

Table 3 shows the aerosol size, refractive index, and humidity information used to calculate the reflectances for each table. These are tailored to the aerosol species simulated by the GOCART model. For dust we examined the range of total column effective radius in the GOCART model and chose three locations: one was near a dust source in the Sahara and had extremely large effective radius (r_{eff}) of 1.6 μm , the second location had $r_{\text{eff}} = 1.4$ μm , and the third location was over ocean far away from the source with $r_{\text{eff}} = 1.0$. The actual radiative transfer calculations use the size distribution from GOCART so they account for particles ranging from 0.1 to 10 μm . The vertical profiles used in the RTC were also taken from GOCART. The refractive indexes are from illite (Querry 1987). For sea salt the reflectances are also dependent on humidity in addition to the dry effective radius. To account for the

TABLE 3. Lookup tables used in forward model for each of the four surface conditions. For pure black carbon index of refraction is $1.75 - 0.45i$. Here BC stands for black carbon and OC stands for organic carbon.

	Effective radius (dry)	Index of refraction	Humidity	Number of tables
Dust small	1.00	$1.414 - 0.0008i$	—	1
Dust medium	1.40	$1.414 - 0.0008i$	—	1
Dust large	1.60	$1.414 - 0.0008i$	—	1
Sea salt small	1.00	$1.490 - 6.0 \times 10^{-8}i$	0%, 80%, 99%	3
Sea salt large	1.30	$1.490 - 6.0 \times 10^{-8}i$	0%, 80%, 99%	3
BC–OC mixture 0.5/0.5	0.042		0%, 80%, 99%	3
BC–OC mixture 0.1/0.9	0.053		0%, 80%, 99%	3
BC–OC mixture 0.02/0.98	0.076		0%, 80%, 99%	3
Pure organic carbon	0.087	$1.53 - 0.005i$	0%, 80%, 99%	3
Sulfate	0.156	$1.430 - 10^{-8}i$	0%, 80%, 99%	3

nonlinear growth factors due to humidity, there are three tables for each effective radius of sea salt and sulfate. Carbonaceous aerosols are treated as mixtures of black and organic carbon. There are three sets of mixtures and a set for pure organic carbon shown in Table 3. All the LUTs of Table 3 assume a surface pressure of 1013 hPa. To account for the effect of surface pressure on the Rayleigh scattering at the smaller wavelength channels, there are two additional tables of Rayleigh radiances assuming 600- and 1040-hPa surface pressure.

To calculate the reflectance from a \mathbf{w}^f vector, an aerosol contribution reflectance is determined for each of the aerosol species: dust, sea salt, hydrophilic carbon, hydrophobic carbon, and sulfate. These species-dependent reflectances, shown in Eq. (5), do not include the reflectance from Rayleigh scattering. For dust the total column mass, and the effective radius is determined based on the four elements of \mathbf{w}^f that pertain to dust, $\text{Dust}_1, \dots, \text{Dust}_4$. The reflectance for dust ρ_{dust} , is interpolated from the two dust tables closest to the effective radius calculated from \mathbf{w}^f . Sea salt interpolates based on relative humidity and dry effective radius. Hydrophilic carbonaceous aerosol interpolates based on black to organic carbon ratio and humidity. Hydrophobic carbonaceous aerosol only uses the dry effective radius. Because the reflectances from the five aerosol types do not include the Rayleigh contribution, they can be summed. The GEOS-DAS provides values of surface pressure so we add an interpolated Rayleigh contribution from 600- and 1040-hPa Rayleigh tables based on the actual surface pressure, ρ_{Rayleigh} :

$$\begin{aligned} \mathbf{h}\mathbf{w}^f = & \rho_{\text{dust}} + \rho_{\text{seasalt}} + \rho_{\text{hydrophobic carbon}} \\ & + \rho_{\text{hydrophilic carbon}} + \rho_{\text{sulfate}} + \rho_{\text{Rayleigh}} \\ & + \rho_{\text{chlorophyll}}. \end{aligned} \quad (5)$$

d. Ocean reflectance

The reflectance of the ocean surface has contributions from sun glint and chlorophyll. The sea surface

BRDF is highly dependent on the surface wind speed and direction. At low wind speeds the surface behaves like a mirror, reflecting heavily in the glint and little outside the glint region. Increasing the wind reduces the disparity between the regions and reflects more light in the off-glint region. Since, surface wind speed values are available from the GEOS-DAS, we can account for this effect using relations derived by Cox and Munk (1954).

The ocean surface reflectance at 0.47, 0.56, and 0.66 μm includes contributions from chlorophyll. We use the relations of Morel (1988) to convert ocean chlorophyll concentration to reflectance and simply include this reflectance as a term in Eq. (5). We obtain our chlorophyll concentrations from a three-dimensional general circulation biogeochemical model described in Gregg (2000, 2002). We opted not to use MODIS-retrieved chlorophyll values from the MODIS ocean color group. In retrieving chlorophyll values the MODIS ocean color group derives their own aerosol optical depths using the 0.66- and 0.87- μm MODIS channels. They convert their derived AOD to an aerosol reflectance for those channels sensitive to chlorophyll, remove this reflectance from the observed value, and attribute the remaining reflectance to chlorophyll. If we use their retrieved chlorophyll, then we run the risk of incorporating their assumptions about aerosols into our analysis.

e. Land surface reflectance

Estimates of the surface reflectance over land are the largest sources of error in our calculated radiances and AOD. Although there are several options available for obtaining surface reflectivity, none is superior. The simplest and the one we use here is the dark target approach used by MAG. If the observed reflectance at 2.13 μm is below a certain value it is deemed a dark target. Empirical measurements show that for dark targets the surface reflectance at 0.47 and 0.66 μm are

constant multiples of the $2.13\text{-}\mu\text{m}$ reflectance. This approach works well over vegetated land surfaces but is inappropriate for other surfaces, bare soils in particular. A second approach is to use the MODIS-filled land surface albedo product for black-sky conditions. These are generated from the official *Terra*/MODIS-derived land surface albedo product, MOD43B3. Values are available at the MODIS channels we are assimilating. However, any calculation of surface reflectivity from satellite radiances requires information about the aerosol optical depth. This sets the stage for a potentially incestuous relationship between the surface reflectivity and the aerosol optical depths, unless they are calculated simultaneously. Since the MODIS-filled land surface albedo product indirectly uses the MAG AOD retrievals in their calculation, our assimilated aerosol optical depths will likely be influenced by the MAG AOD retrievals.

3. Results—GOCART retrievals

We can tune the GOCART model error-covariance matrix so that the GOCART retrieval AOD best matches the Aerosol Robotic Network (AERONET) observations. The primary objective of the tuning is to adjust the GOCART model error-covariance matrix so that the analysis and observed radiances closely match, especially at the $0.87\text{-}\mu\text{m}$ channel over ocean and at the $0.47\text{-}\mu\text{m}$ channel over land. An additional objective is to keep the analysis species distribution similar to the GOCART distribution. In other words, usually we want the analysis to remember some of the species distribution information from the GOCART model. The error-covariance matrix coefficients that yield a retrieved AOD that best matches the AERONET observations are shown in Tables 1 and 2. Once the analysis module is tuned to our satisfaction we will turn on the cycling and perform an assimilation (section 4). Since the AERONET observations are point measurements, we only use MODIS radiances in $0.5^\circ \times 0.625^\circ$ box when comparing with the ground-based observations. Tuning with retrievals allows us to retrieve only at the AERONET locations. Tuning the error-covariance matrix during the assimilation cycle turned requires analysis at every GOCART grid point and would be much slower.

a. Issues with black carbon

An analysis is performed when MODIS reflectances are available within a GOCART $2^\circ \times 2.5^\circ$ grid box. Results from mixture of carbonaceous and dust aerosols observed off the coast of Madagascar over a rough

ocean surface are shown in Fig. 2. The top and lower-left panels are the MODIS observations (black dots), the first guess (blue trace), and the analysis (red trace) reflectances plotted against appropriate LUT (green traces). The LUT of the dominant aerosol (organic carbon) shows that the reflectance seen by the satellite increases with increasing dust optical depth. Loading the atmosphere with any nonabsorbing aerosol back scatters more radiance toward the satellite.

The second most dominant aerosol type (black carbon) is highly absorbing and shows reduced reflectance with increased black carbon loading at the shortest frequencies. Including a black carbon LUT in the analysis complicates matters because its effect on the radiances is counter the effect of the other LUTs, which are nonabsorbing at all channels. Left unconstrained, the analysis will eliminate the contribution from black carbon aerosol and sometimes even yield negative values of aerosol mixing ratio. Since leaving the black carbon unconstrained leads to unstable results, we significantly reduce the GOCART model error covariance for black carbon (Table 1). This only allows a small deviation of black carbon values from the first-guess GOCART value.

The third most dominant aerosol (dust) is also nonabsorbing but has flatter radiances with changing frequency compared with the organic carbon. Generally, aerosols with larger effective radii will have flatter spectral signature (the change in radiances with changing frequency), compared with smaller aerosols that will have a steeper signature. In our analysis and in the MAG retrieval the spectral signature in the observed MODIS radiances over ocean can distinguish between the large and small aerosol types, but it cannot provide information about the type of large particle (dust or sea salt) nor the type of small particle (carbon or sulfate). In our analysis the GOCART model provides this information.

The analysis finds the combination of the LUTs that best fits the MODIS observations while minimizing changes to the first-guess GOCART concentrations. Here the GOCART model clearly forecasts too much aerosol, since the first-guess reflectances (blue trace) are above the observed (black dots). The analysis removed aerosol to minimize the difference between the observed and analyzed reflectance. The analysis significantly reduces the amount of sulfate aerosol from the first-guess values to reduce the reflectances at all channels and retains the amount of larger particles to fit the shape of the observations. For this case the analysis total AOD value is slightly more than the retrieved AOD from the MAG retrieval group. Over ocean sur-

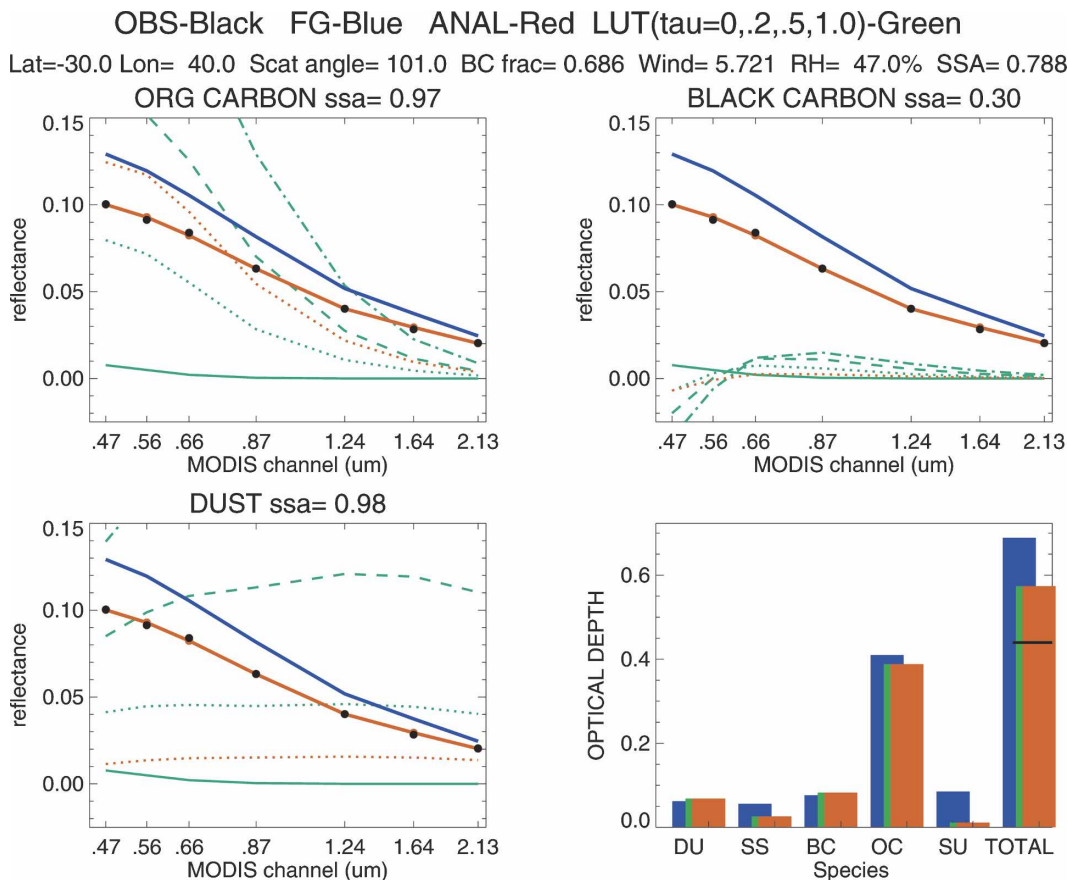


FIG. 2. Results from an analysis of a single grid point over ocean. (top), (bottom left) Reflectances minus the Rayleigh component: MODIS-observed level-2 reflectances (black dots), first-guess reflectances from the forward model (blue solid trace), analysis reflectances (red solid line). The reflectances from the LUT of (left) the primary aerosol species (organic carbon) is plotted, and (right) for the second dominant species (black carbon) and (bottom left) the third dominant species (dust). These are shown for the appropriate MODIS satellite viewing geometry, surface wind speed, and relative humidity. Shown are Rayleigh reflectances (green solid line), reflectances at AOD = 0.2 (green dotted line), AOD = 0.5 (green dashed line), AOD = 1.0 (green dashed-dotted line). The AOD of the aerosol species of the LUT are also shown (red dotted line). (bottom right) Species distribution in terms of AOD. First guess is denoted by blue bars, second guess by green, and analysis by red bars. (lower right) The black bar is the AOD retrieved by the MODIS atmosphere working group.

faces the analysis is usually able to closely match all reflectances.

Figure 3 shows the analysis over a sufficiently dark target land surface at the Abracos Hill AERONET site in central Brazil. The first-guess reflectances (blue) are less than the observed values (black dots). Over this relatively dark site, adding nonabsorbing organic carbon to the first guess will increase the reflectance while adding absorbing black carbon will cause a decrease. Left unconstrained the analysis could match the observations with unrealistically large amounts of both nonabsorbing and absorbing aerosol. Fortunately the deviation between the analysis the first guess state vector is minimized [first term of Eq. (1)], which prevents unrealistic solutions. Still observations at the 0.47- and

0.66- μm channels cannot determine the ratio of absorbing to nonabsorbing aerosol so we must rely on information from the GOCART model.

b. AERONET

AERONET (described by Holben et al. 2001) is an optical ground-based aerosol monitoring network designed to validate satellite aerosol measurements. The hardware consists of identical automatic sun-sky scanning spectral radiometers that are placed nearby known source regions, in populated areas, and in remote environments. The network of radiometers is intercalibrated and provides column-integrated AOD measurements several times a day; some sites have data for 10 yr. The AOD values used here are level-2.0 values,

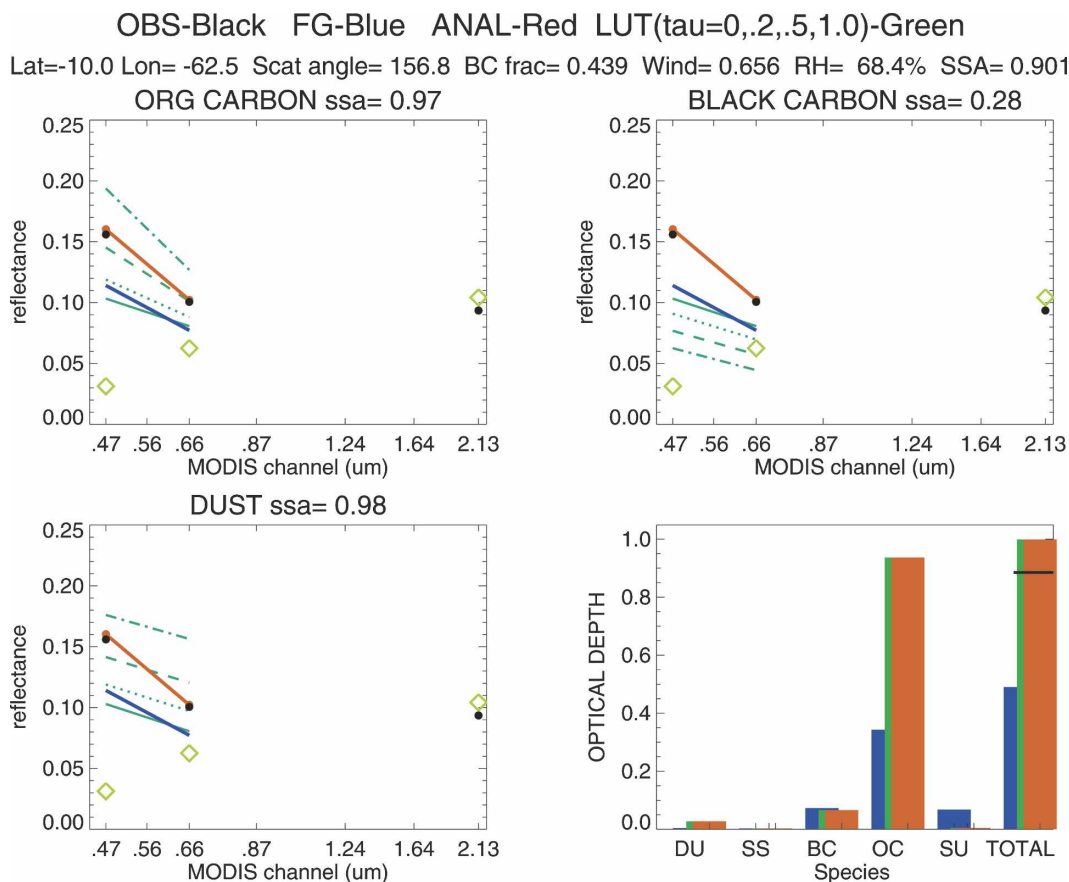


FIG. 3. Results from an analysis of a single grid point over land at the Abracos Hill AERONET site. The color coding is the same as in Fig. 2; however, the actual reflectances are shown. The open diamond at $2.13 \mu\text{m}$ is the MODIS-observed reflectance minus the absorption due to atmospheric gases and dust. This open diamond is used to calculate the surface reflectance at 0.47 and $0.66 \mu\text{m}$ (also shown by open diamonds) using the dark target approach.

which are cloud screened and quality assured (manually checked for anomalous values). A new inversion algorithm (Dubovik et al. 2002; Dubovik and King 2000) provides single-scattering albedo using the full suite of sun and sky radiances for the almucanter and solar principle plane. Since the uncertainty in retrieved single-scattering is largest for light aerosol loading conditions, we only use retrieved single-scattering values during when $\text{AOD} > 0.2$ for our comparisons.

Our results and MAG retrievals are compared with the AERONET data at selected stations in Figs. 4,5. The time series of the four AERONET sites that usually have nearby ocean MODIS radiances (Fig. 4) show that both our AOD analysis (red points) and MAG retrievals (black points) compare equally well with the AERONET data. Both our analysis and the MAG retrievals are able to capture episodes of high aerosol loading. For example the high AOD seen by the AERONET during early to mid-August (Julian day

220–235) at the Clouds and Earth’s Radiant Energy System (CERES) Ocean Validation Experiment (COVE) site and an episode in late August (Julian day 240) at Dry Tortugas are captured by both satellite products.

Our analysis and MAG retrievals also show good agreement with a time series of AERONET AOD at two sites in central Brazil (upper panels of Fig. 5). Both our analysis and AERONET retrieved single scattering albedo ω_o (lower panel of Fig. 5) seem to be correlated with the AOD. Even though Reid and Hobbs (1998) measure $\omega_o < 0.4$ on several occasions from grass fires in Brazil, our low ω_o values are highly uncertain because of the low AOD levels. We can say that our analysis and the AERONET ω_o retrieval choose to use more absorbing aerosol in the solution at low AOD than during the high loading episodes. This relationship is striking at the Cuiaba-Miranda site and less so at Abracos Hill. The low ω_o indicates that savanna grasses

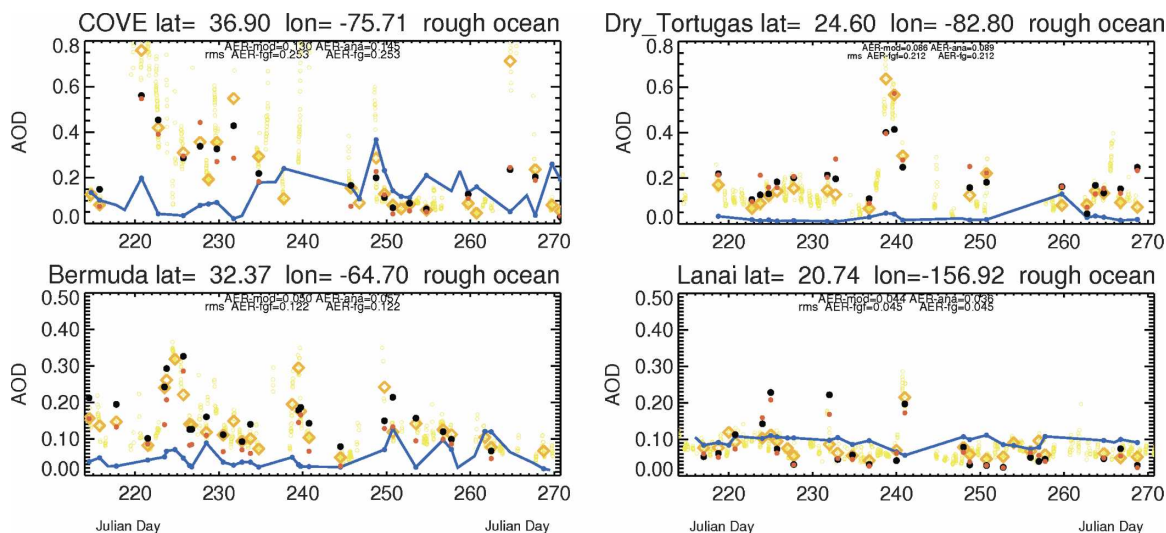


FIG. 4. Time series of AOD for four AERONET stations near ocean: COVE, Bermuda, Dry Tortugas, and Lanai. The AERONET data may have several measurements per day and are shown by faint yellow circles. For a given AERONET location, MODIS radiances, and MAG retrievals are usually available only once per day during daylight hours. The yellow diamonds are the average of the morning AERONET retrievals. The black points are AOD from the MAG retrievals averaged over the $0.5^\circ \times 0.625^\circ$ grid box nearest to the AERONET site. Red points are our GOCART-retrieval AOD values usually reported once per day and blue are our first-guess values reported 4 times per day. If the GOCART retrieval uses the MODIS ocean radiances and a surface reflectance based on a rough ocean, the MAG retrievals and our GOCART retrievals are shown as solid circles. If MODIS land radiances are used the retrievals are shown as squares. The latitude, longitude, and surface reflectance properties are also shown.

were the primary fuel that produced the aerosol, while higher ω_0 is indicative of deforestation. Ward et al. (1992, 1996) found distinct differences in the black carbon content of aerosols from fires of savanna ecosystems and fires of burning rain forests. Dry savanna grasses burn at high flame temperatures producing significant amounts of absorbing black carbon. Rain forests burn (actually smolder) at a lower temperature and

produce aerosol that is less absorbing. Since, Cuiaba-Miranda is surrounded by dry savanna grass, it is likely that the low AOD events are from local fires that would produce significant amounts of black carbon. The higher AOD events may be from deforestation fires from the north of Cuiaba that have lower black carbon production. (Eck et al. 1998).

The retrieval is able to digest information from the

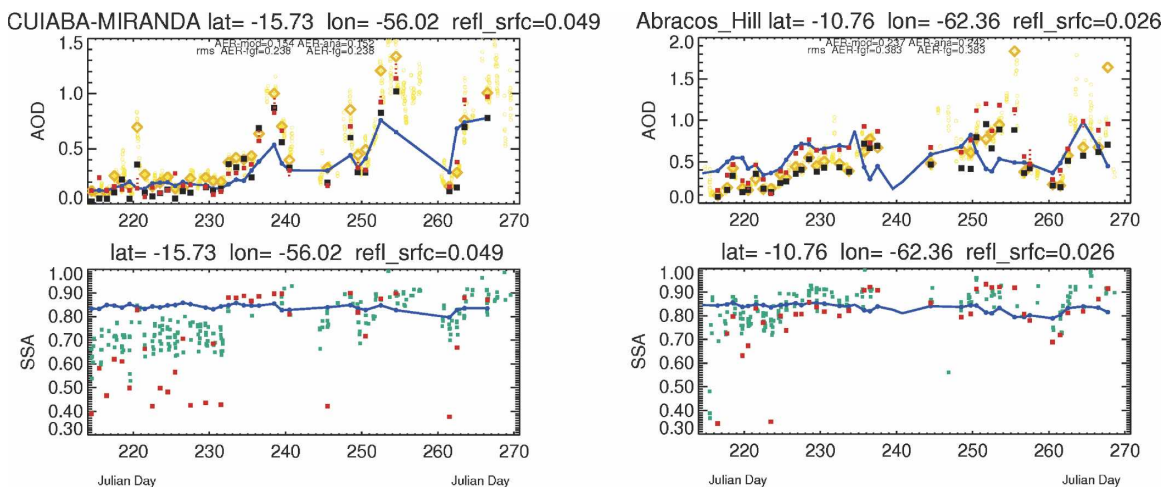


FIG. 5. Time series of (top) AOD and (bottom) single-scattering albedo (SSA) for two AERONET stations in central Brazil. Cuiaba-Miranda and Abracos Hill use the same color scheme as Fig. 4. Lower panel shows the time series of AERONET SSA observations (green squares) and the GOCART-retrieved SSA (red squares).

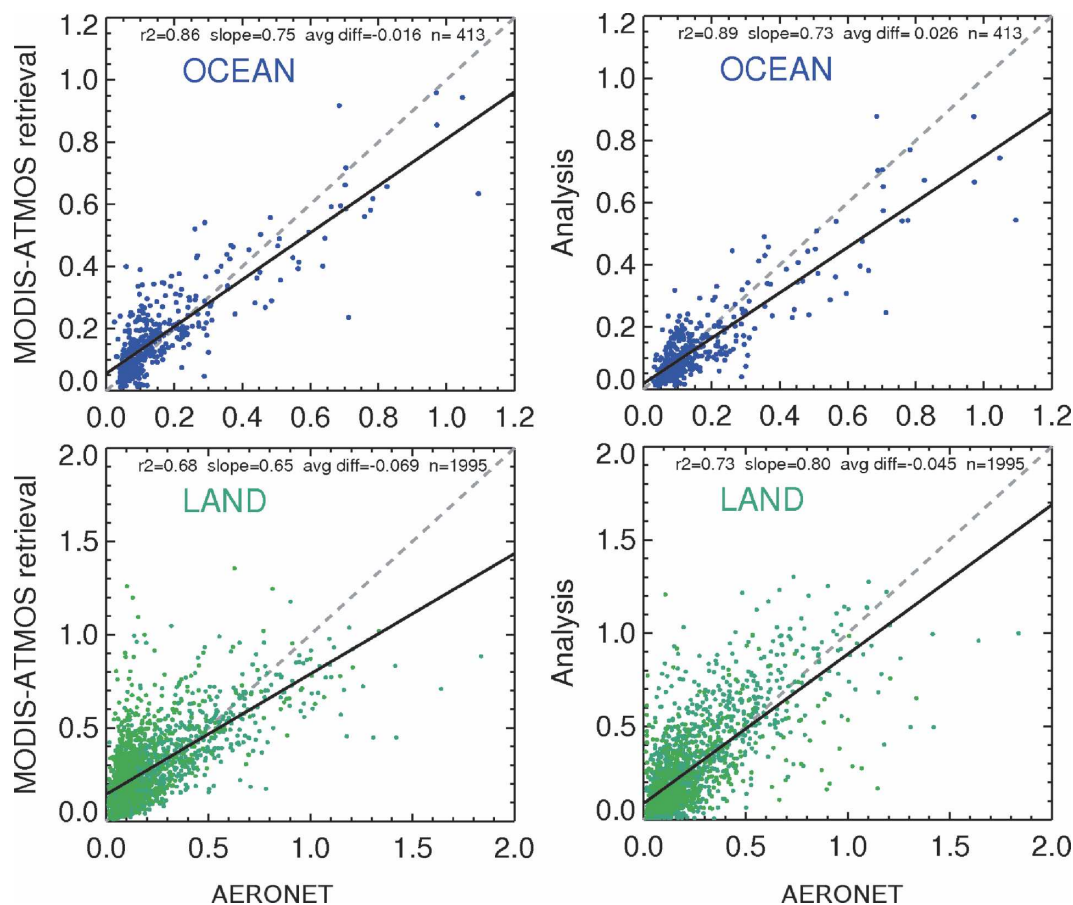


FIG. 6. MAG AOD retrieval (version 4) and our GOCART retrieval (analysis) regressed against AERONET values for July–September 2001. The top legend on each panel shows the squared correlation coefficient, the slope, the mean difference between the plotted quantities “avg diff,” and the total number of points plotted. The “avg diff” is a measure of the bias between the plotted quantities.

MODIS radiance and the GOCART model to provide information on the AOD and the ω_o , which is not currently possible from the MODIS radiances alone. Over land the MODIS radiances provide only one piece of information (the radiance at $0.47 \mu\text{m}$) to the analysis solution. Information about the amount of absorbing aerosol is provided by the GOCART. (Recall the analysis black carbon value is constrained by GOCART.)

The MAG retrievals and our analysis are regressed against the AERONET AOD in Fig. 6. The July to September 2001 period was chosen because there were several significant Saharan dust events that caused high aerosol loading over the tropical Atlantic; also there was significant loading from biomass burning over Brazil and significant loading off the South African coast. Over ocean, both satellite-derived products compare well against the AERONET AOD. Over land, both satellite products fail to simulate the AERONET for high loading condition, although our analysis does a

slightly better job. The AOD for these errant points are often dominated by biomass burning. The red circled point is the analysis solution over Abracos Hill discussed in Fig. 3. In that case, both satellite products estimated an AOD of about 1 but the AERONET observed 1.8. We suspect that the both satellite products are not including enough black carbon in their solution.

Doubling the amount of black carbon assumed in GOCART increases the retrieved AOD. For some sites, like Abracos Hill, this improves the comparison with AERONET AOD. But doubling black carbon degrades the overall global comparison with AERONET AOD and single-scattering albedo. Most of the improvement in our analysis is at locations over moderately light surfaces that are composed of soil rather than dark vegetation. Most of the AERONET sites in the western United States fit this description. At moderately bright locations the estimated surface reflectance, which is based on a multiple of the observed

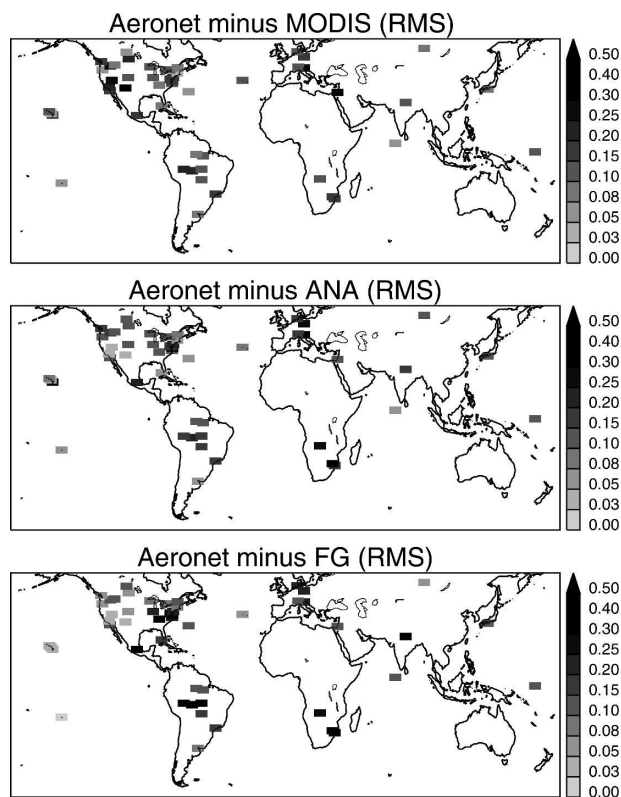


FIG. 7. Root-mean-square error for AERONET minus (top) MAG AOD, (middle) our GOCART retrieval (analysis), and (bottom) our first-guess for July–September 2001.

2.13- μm reflectance, is often too high and will cause a positive bias in the retrieved AOD. Cases of moderately light surfaces (surface reflectance >0.15) are shown as light points in Fig. 6. Our analysis draws to the GOCART model, rather than the observed MODIS radiances, when the observed 2.13- μm reflectance senses that the underlying surface is not a vegetative dark target. The MAG retrieval does not have the luxury of reverting to estimates from an aerosol-transport model and must use the uncertain surface reflectance. Figure 7 shows the spatial distribution of the deviation (the RMS error) between the MAG, our analysis (GOCART retrieval), and our first-guess AOD compared with AERONET. Over the western United States, the MAG-retrieved AOD is often in error by more than 0.10 or more. The error for the GOCART first-guess values in the western United States is much less (Fig. 7, bottom panel). Elsewhere our analysis seems to be as good as the MAG retrievals except for sites in southern Africa.

Figure 8 shows the ω_o comparison. Over ocean the correlation coefficient is significant ($r^2 = 0.41$) and indicates that the black carbon levels in the solution

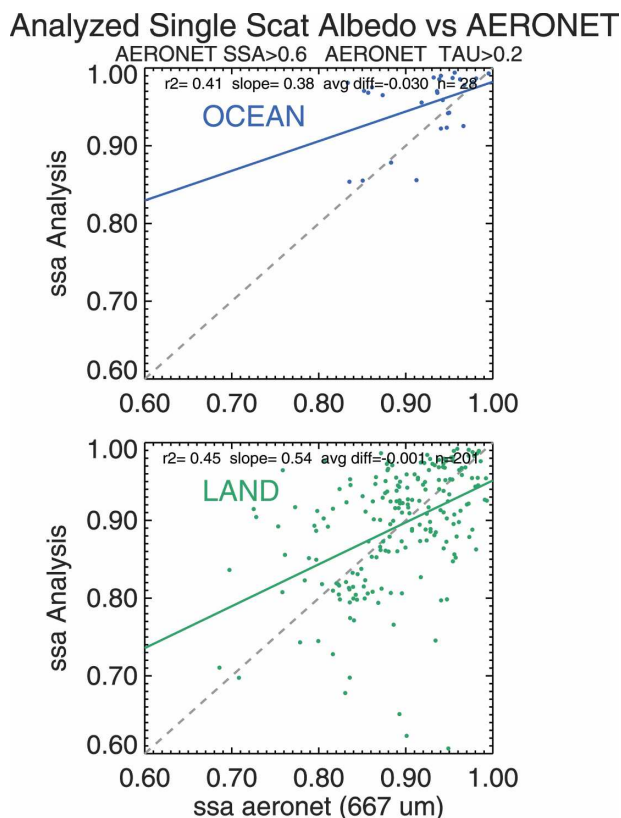


FIG. 8. Single-scattering albedo from the GOCART retrieval (analysis) regressed against AERONET values for July–September 2001.

are reasonable. Because there are so few coastal AERONET stations with significant AOD (>0.2) it is difficult to further evaluate our ω_o product. The MAG ω_o is not available for comparison; however, none of the aerosol models used in the MAG retrieval over ocean are very absorbing, the lowest ω_o is 0.97 for dust. Therefore, the MAG ω_o over ocean would not be able to reproduce the AERONET observations. Over land our analysis uses information from only one MODIS channel (0.47 μm). Any correlation between AERONET and the GOCART retrieval over land is from the aerosol species distribution provided by the GOCART model.

4. Results—Assimilation

The first-guess concentrations for the GOCART retrieval system were from a free-running GOCART model; MODIS information was never inserted. We now present results with the assimilation cycle turned on. At those GOCART grid points where MODIS radiances are available the first-guess aerosol concentra-

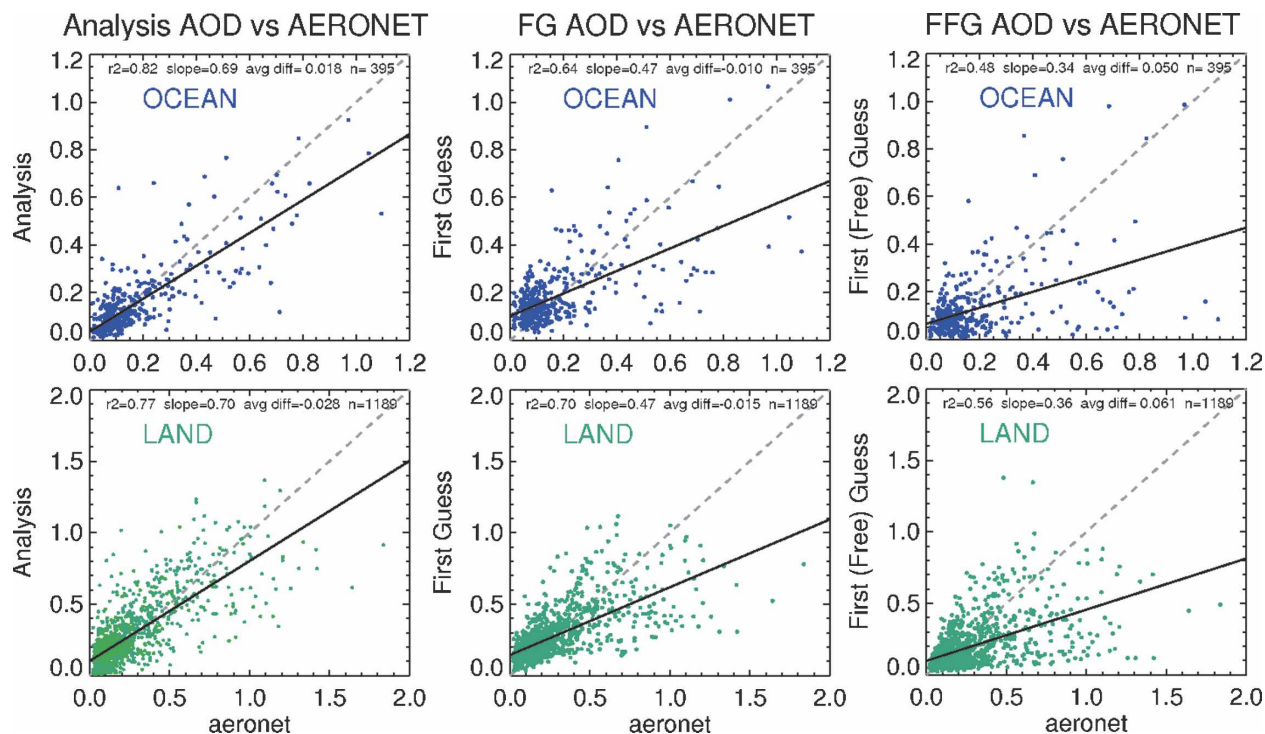


FIG. 9. Three AOD products from our assimilation system regressed against the AERONET data for August–September 2001. (left) Analysis AOD from the assimilation, (middle) assimilation first guess, and (right) the first guess from a GOCART retrieval at coarse horizontal resolution. All products are produced using a $2^{\circ} \times 2.5^{\circ}$ grid.

tions, w^f , are being replaced by the analysis concentrations, w^a . (The dashed arrow in Fig. 1 is activated.)

We compare the assimilation results with the AERONET observations with the understanding that

coarse resolution used in the assimilation will not be able to simulate some of the high AOD values seen by AERONET. Figure 9 shows the AERONET AOD compared with products with different levels of MODIS

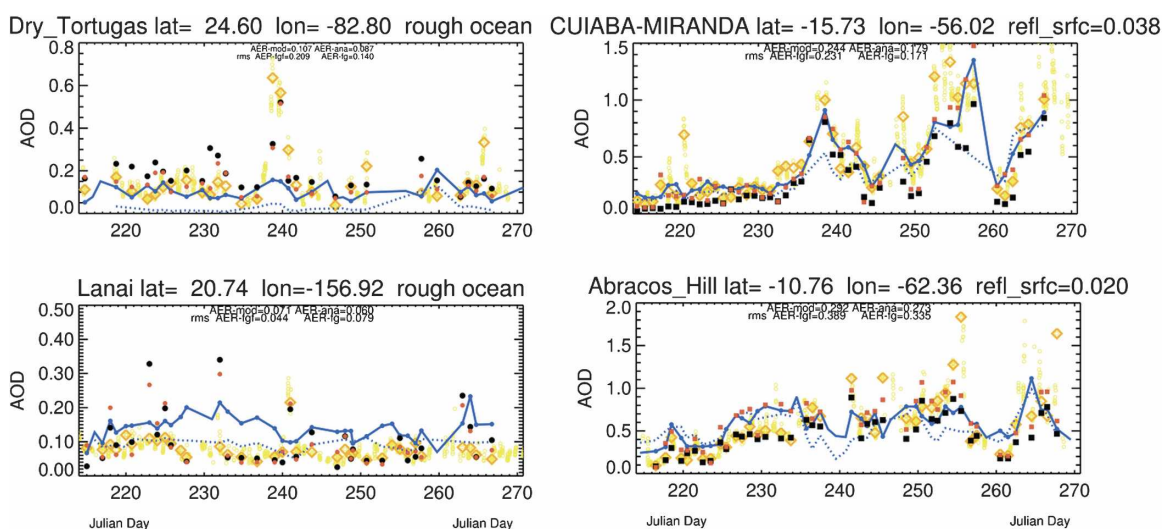


FIG. 10. Time series of AOD for two AERONET stations in central Brazil: Cuiaba-Miranda and Abracos Hill. The AERONET data may have several measurements per day and are shown by faint yellow circles. For a given AERONET location, MODIS radiances, and MAG retrievals are usually available only once per day during daylight hours. The yellow diamonds are the average of the morning AERONET retrievals. The black points are AOD from the MAG retrievals averaged over the $2^{\circ} \times 2.5^{\circ}$ grid box nearest to the AERONET site. Red points are our analysis values from the assimilation usually reported once per day. Solid blue trace is our first-guess values reported 4 times per day. The dotted blue trace is the first guess from the GOCART retrieval run at $2^{\circ} \times 2.5^{\circ}$ resolution.

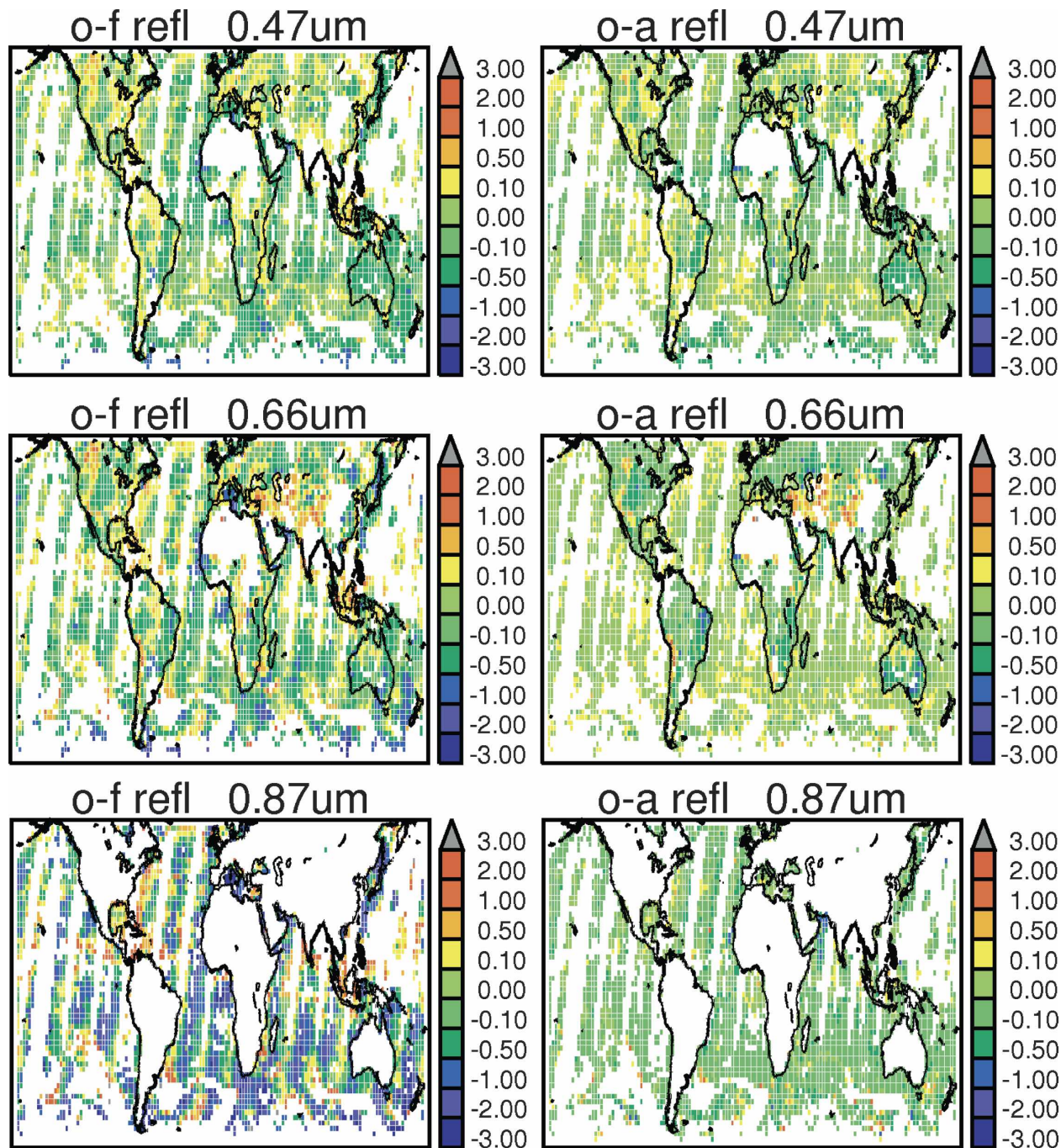


FIG. 11. Fractional error (left) $(O - F)/O$ and (right) $(O - A)/O$ for three channels 0.47, 0.66, and 0.87 μm for 18 Aug 2001; O is observed reflectance, F is the assimilation first-guess reflectance, and A is assimilation analysis reflectance.

information. On the left panel AERONET is regressed with AOD from the analysis of the assimilation run at coarse ($2^\circ \times 2.5^\circ$) resolution. Since the analysis aerosol concentrations have just been adjusted to agree with the MODIS radiances, the analysis AOD has the highest level of MODIS information content. On the middle panel, AERONET is regressed with AOD from the

first guess of the assimilation. The first guess has only a moderate level of MODIS information, since it was inserted 24 h ago. The first-guess regression with AERONET is not as good as the analysis because the aerosol concentrations have started to return to the values of the free-running GOCART. On the right panel AERONET is regressed with AOD from the first guess

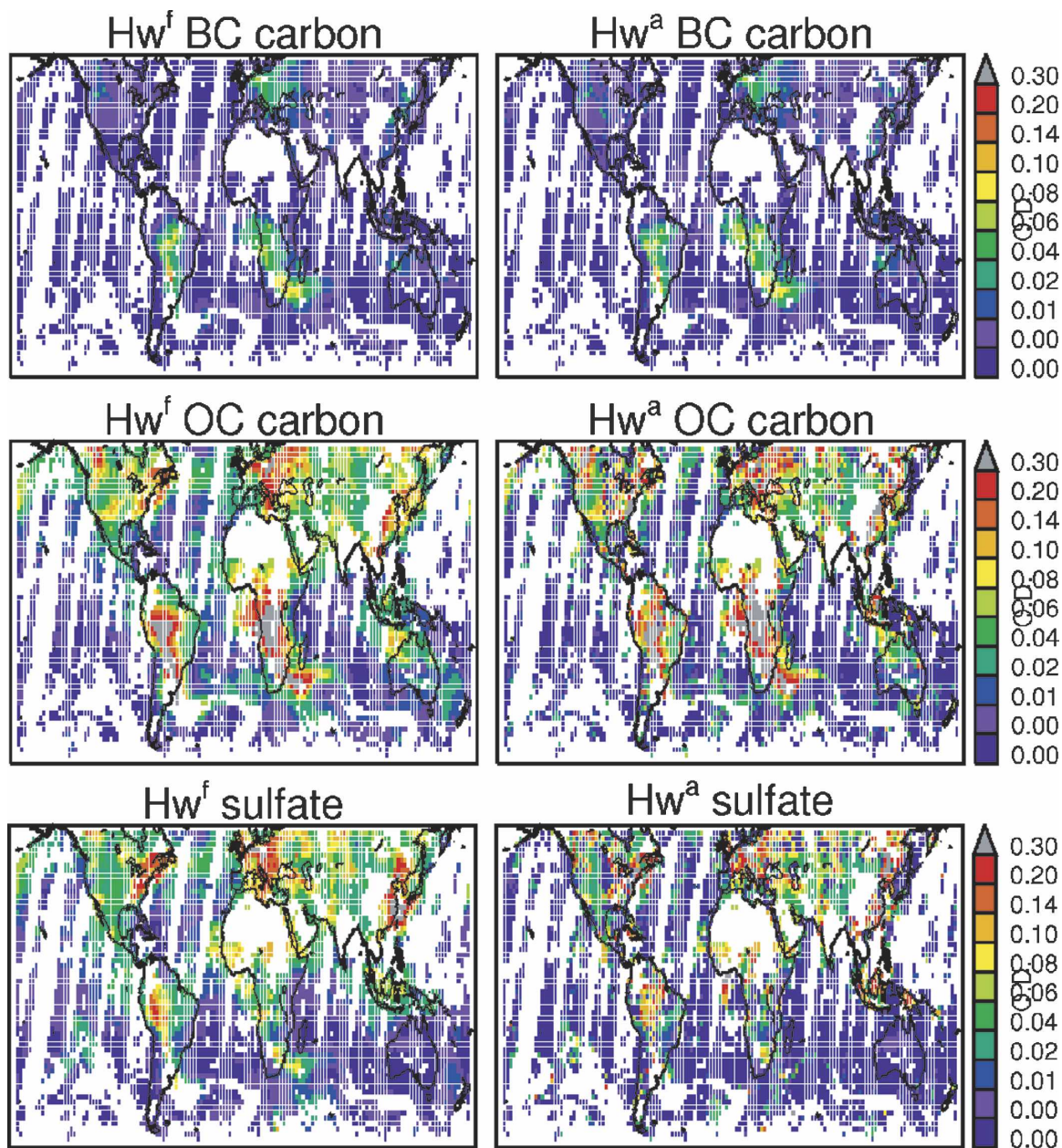


FIG. 12. AOD of five different aerosol species simulated by the assimilation for a single day, (left) the first guess from the assimilation and (right) the analysis.

of a free-running GOCART MODEL run at coarse ($2^\circ \times 2.5^\circ$) resolution. Since the GOCART is free running, there has never (nor will there ever be) any MODIS information insertion. These panels show that the more recent the time of the MODIS information insertion, the better the comparison with the AERONET AOD. It is significant that the assimilation first guess is closer to the AERONET compared with the free-running first guess. This indicates that the MODIS information is being retained in the GOCART model

even after 24 h. An identical performance between the assimilation first guess and the free-running GOCART would indicate that the MODIS information was not being retained after 24 h.

The differences between the analysis and first guess for a mature assimilation system in tandem with an accurate forward model will be small. Since the forecast model will accurately simulate the atmospheric state to the time when the next observations are available, there will be little difference between the analysis and

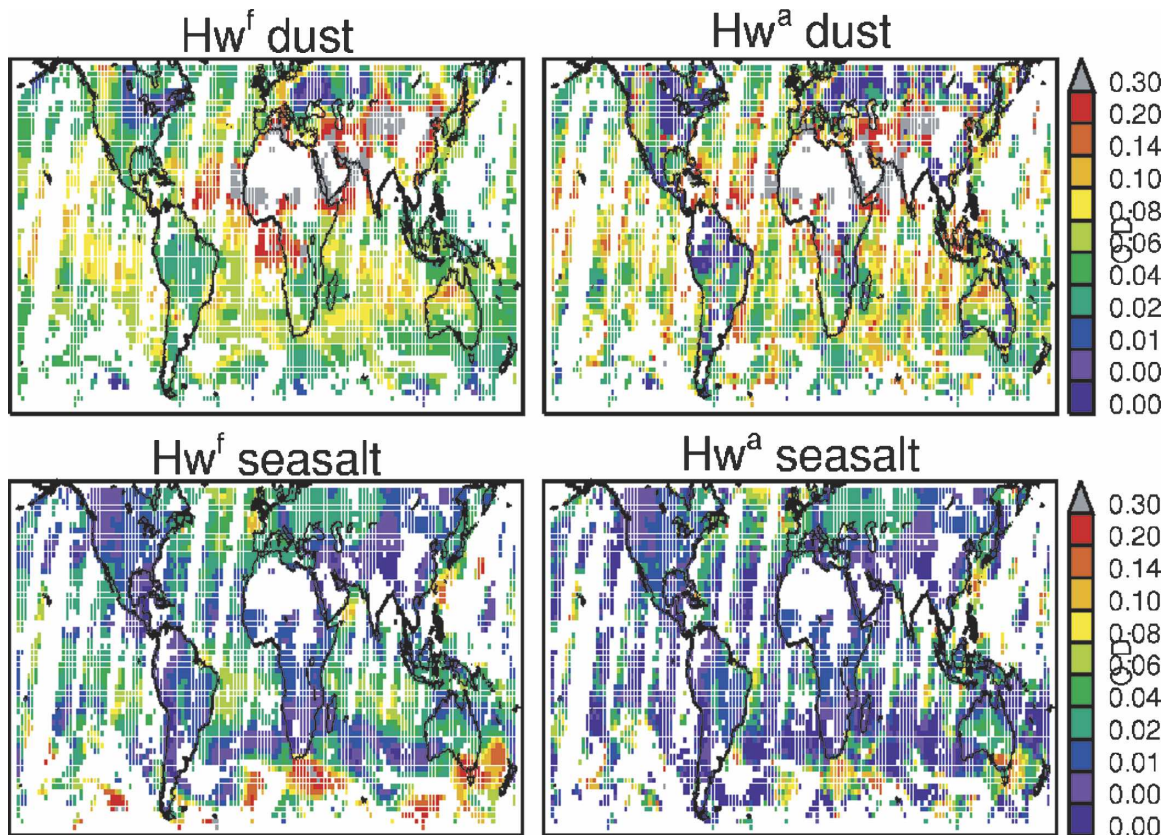


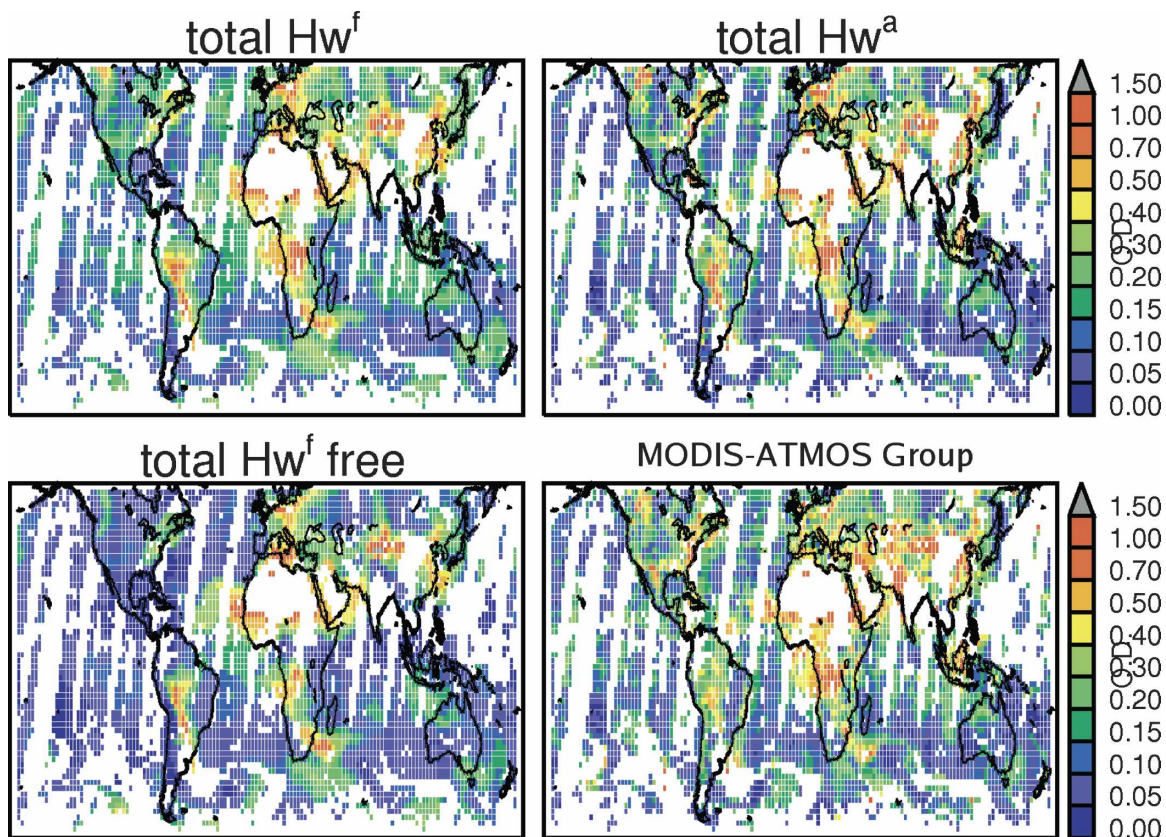
FIG. 12. (Continued)

the forecast concentrations. A time series of these products at selected AERONET sites is shown in Fig. 10. At Dry Tortugas the insertion of MODIS information draws the assimilation first guess closer to the AERONET than the free-running GOCART. This behavior indicates the MODIS information is being retained in GOCART at least in this region; at Lanai, insertion of MODIS information draws the GOCART model away from the lower AERONET observations. Over land, MODIS information improves the GOCART model performance during strong loading events at Cuiaba-Miranda but at Abracos Hill the impact is mixed.

We can also evaluate the assimilation system by comparing the first-guess and analysis radiances with the observed radiances. Figure 11 shows global plots of the fractional error for a single day. Over ocean for all channels shown, analysis module is almost always drawing to the observed radiances since the fractional error is always less for the analysis compared with the first guess. Recall that the observational error covariance matrix is designed to draw closest to the $0.87\text{-}\mu\text{m}$ channel over ocean and to the $0.47\text{-}\mu\text{m}$ channel over land (Table 2). The differences between the observed and

the analysis radiances are smallest at the $0.87\text{-}\mu\text{m}$ channel over ocean and $0.47\text{ }\mu\text{m}$ over land. This is consistent with the observational error covariance matrix and indicates that the analysis module is working properly. On the other hand, the observed minus forecast radiances are significant and indicate that there is room for improvement in either our radiative transfer model or the GOCART model (probably both).

We want to make sure that the spatial distributions of the individual species are realistic. An improperly tuned analysis module could mistake dust for sea salt over far inland locations and yield unrealistic results. Figure 12 shows global AOD plots of the different aerosol species from the assimilation first guess and the analysis for a single day. The analysis maintains the same realistic-looking spatial distribution as the GOCART first guess while matching the MODIS radiances. All species are allowed to deviate from the first-guess values except for black carbon. We had to reduce the estimates for the error covariance in the first-guess black carbon concentrations to insure a stable analysis module. This keeps the values for the analysis from deviating too far from the first guess. Figure 13 shows global distributions of the total AOD from the first guess and



GAAS.STD.tv12.anal2. 20010818

FIG. 13. AOD of total aerosol optical depth for a single day. (top left) The assimilation first guess, (top right) the assimilation analysis, (bottom left) the free-running GOCART model, and (bottom right) the MAG retrieval.

analysis of the assimilation system, the free-running GOCART, and finally the MAG-retrieved AOD. The difference between the analysis and the free-running GOCART model shows the impact of inserting the MODIS radiance information. The dust plume over the tropical Atlantic off the coast of Africa is reduced by drawing to the MODIS radiances. The AOD over the biomass-burning regions in South America are relatively unchanged, but over tropical Africa the AOD is significantly increased.

5. Discussion

We have presented results from a retrieval and assimilation system of MODIS radiances that are sensitive to aerosols. We use the AERONET aerosol optical depth (AOD) observations as a yardstick since they are our best estimate of the true atmospheric aerosol loading.

We wanted to test whether the GOCART model offers information about the aerosol spatial distribution

and optical properties that are an improvement to the assumptions used by traditional retrieval methods. If so, then our GOCART retrievals should compare better with the AERONET than the MAG retrievals do. Although this is the case (see Fig. 6), most of our improvement is simply because we do not try to assimilate the MODIS radiance over bright surfaces. In these cases we simply use the GOCART AOD. At this time we cannot claim a significant improvement in AOD over traditional retrieval methods. Our retrieval also provides single-scattering albedo (ω_o) values, which show reasonable correlation with AERONET over ocean. Although the correlation is poorer over land, we show a case where the combination of the GOCART and the radiances yields ω_o that is qualitatively in agreement with AERONET.

We also wanted to test whether insertion of MODIS radiances brings the GOCART model in closer agreement to the AERONET observations. The results from the assimilation shown in Fig. 9 definitely show an improvement when the radiances are inserted.

However, too often neither our AOD satellite products nor the MAG retrievals are able to attain the high AOD observations seen by AERONET. This could be due to not including enough absorbing aerosol in the analysis solution. We need to improve our estimates of the ω_0 , since they are just as important as AOD when calculating radiative forcing. On the other hand, at low AOD our satellite products and MAG retrievals are too high compared with AERONET both over land and ocean.

The goal of the GAAS is to provide the scientific community with complete global coverage 3D fields of aerosol. This unique product will be consistent with satellite radiances yet be differentiated by aerosol species. Once the individual species are validated by ground observations, we can use them to study radiative forcing.

Acknowledgments. We thank the Yoram Kaufman for helpful discussions, David Giles for making the AERONET data available. This work is supported by the NASA Office of Earth Science: Earth System Science Research using data products from *Terra*, *Aqua*, and *ACRIM* satellites. Results will be available on the back trajectories, AERONET, MODIS, GOCART, MPLNET Aerosol Synergism (BAMGOMAS) Web site.

REFERENCES

- Chin, M., and Coauthors, 2002: Tropospheric aerosol optical thickness from the GOCART model and comparisons with satellite and sunphotometer measurements. *J. Atmos. Sci.*, **59**, 461–483.
- , D. A. Chu, R. Levy, L. A. Remer, Y. J. Kaufman, B. N. Holben, T. Eck, and P. Ginoux, 2004: Aerosol distribution in the Northern Hemisphere during ACE-Asia: Results from global model, satellite observations, and sunphotometer measurements. *J. Geophys. Res.*, **109**, D23S90, doi:10.1029/2004JD004829.
- Collins, W. D., P. J. Rasch, B. E. Eaton, B. V. Khatatov, J.-F. Lamarque, and C. S. Zender, 2001: Simulating aerosols using a chemical transport model with assimilation of satellite aerosol retrievals: Methodology for INDOEX. *J. Geophys. Res.*, **106**, 7313–7336.
- Cooke, W. F., C. Liou, H. Cachier, and J. Feichter, 1999: Construction of a 1x1 degree fossil fuel emission data set for carbonaceous aerosol and implementation and radiative impact in the ECHAM-4 model. *J. Geophys. Res.*, **104**, 22 137–22 162.
- Cox, C., and W. Munk, 1954: Measurement of the roughness of the sea surface from photographs of the Sun's glitter. *J. Opt. Soc. Amer.*, **44**, 838–850.
- Dubovik, O., and M. King, 2000: A flexible inversion algorithm for retrieval of aerosol optical properties from Sun and sky radiance measurements. *J. Geophys. Res.*, **105**, 20 673–20 696.
- , B. Holben, T. F. Eck, A. Smirnov, Y. J. Kaufman, M. D. King, D. Tanre, and I. Slutsker, 2002: Variability of absorption and optical properties of key aerosol types observed in worldwide. *J. Atmos. Sci.*, **59**, 590–608.
- Duncan, B. N., V. M. Randall, A. C. Staudt, R. Yevich, and J. A. Logan, 2003: Interannual and seasonal variability of biomass burning emissions constrained by satellite observations. *J. Geophys. Res.*, **108**, 4040, doi:10.1029/2002JD002378.
- Eck, T. F., B. N. Holben, I. Slutsker, and A. Setzer, 1998: Measurements of irradiance and attenuation and estimation of aerosol single-scattering albedo for biomass burning aerosols in Amazonia. *J. Geophys. Res.*, **103**, 31 865–31 878.
- Gatebe, C. K., M. D. King, S. Platnick, G. T. Arnold, E. F. Vermote, and B. Schmid, 2003: Airborne spectral measurements of surface-atmosphere anisotropy for several surfaces and ecosystems over southern Africa. *J. Geophys. Res.*, **108**, 8489, doi:10.1029/2002JD002397.
- Ginoux, P., M. Chin, I. Tegen, J. M. Prospero, B. Holben, O. Dubovik, and S. J. Lin, 2001: Sources and distributions of dust aerosols simulated with the GOCART model. *J. Geophys. Res.*, **106**, 20 225–20 273.
- Gregg, W. W., 2000: A coupled ocean general circulation, biogeochemical, and radiative model of the global oceans: Seasonal distributions of ocean chlorophyll and nutrients. NASA Tech. Memo. 2000-209965, 33 pp.
- , 2002: Tracking the SeaWiFS record with a coupled physical/biogeochemical/radiative model of the global oceans. *Deep-Sea Res. II*, **49**, 81–105.
- Holben, B. N., and Coauthors, 2001: An emerging ground-based aerosol climatology: Aerosol optical depth from AERONET. *J. Geophys. Res.*, **106**, 12 067–12 097.
- Herman, B. M., and S. R. Browning, 1965: A numerical solution to the equation of radiative transfer. *J. Atmos. Sci.*, **22**, 559–566.
- Kopke, P., M. Hess, I. Schult, and E. P. Shettle, 1997: Global aerosol data set. Tech. Rep. 243, Max Planck Institute, 44 pp.
- Lin, S.-J., and R. B. Rood, 1996: Multidimensional flux-form semi-Lagrangian transport schemes. *Mon. Wea. Rev.*, **124**, 2046–2070.
- Martin, R. V., D. J. Jacob, R. M. Yantosca, M. Chin, and P. Ginoux, 2003: Global and regional decreases in tropospheric oxidants from photochemical effects of aerosols. *J. Geophys. Res.*, **108**, 4097, doi:10.1029/2002JD002622.
- Monahan, E. C., D. E. Spiel, and K. L. Davidson, 1986: A model of marine aerosol generation via whitecaps and wave disruption. *Oceanic Whitecaps*, E. C. Monahan and G. Mac Niocaill, Eds., D. Reidel, 167–174.
- Morel, A., 1988: Optical modeling of the upper ocean in relation to its biogenous matter content (case I waters), 1988. *J. Geophys. Res.*, **93**, 10 749–10 768.
- Nalli, N. R., and L. L. Stowe, 2002: Aerosol correction for remotely sensed sea surface temperatures from the National Oceanic and Atmospheric Administration advanced very high resolution radiometer. *J. Geophys. Res.*, **107**, 3172, doi:10.1029/2001JC001162.
- Querry, M. R., 1987: Optical constants of minerals and other materials from the millimeter to the UV. Rep. CRDEC-CR-88009, U.S. Army, 331 pp.
- Ramaswamy, V., and Coauthors, 2001: Radiative forcing of climate change. *Climate Change 2001: The Scientific Basis*, J. T. Houghton et al., Eds., Cambridge University Press, 351–416.
- Reid, J. S., and P. V. Hobbs, 1998: Physical and optical properties

- of young smoke from individual biomass fires in Brazil. *J. Geophys. Res.*, **103**, 32 013–32 031.
- Remer, L. A., and Coauthors, 2005: The MODIS aerosol algorithm, products and validation. *J. Atmos. Sci.*, **62**, 947–973.
- Schubert, S. R., R. B. Rood, and J. Pfaendtner, 1993: An assimilated dataset for earth science applications. *Bull. Amer. Meteor. Soc.*, **74**, 2331–2342.
- Wang, J., U. S. Nair, and S. A. Christopher, 2004: GOES 8 aerosol optical thickness assimilation in a mesoscale model: Online integration of aerosol radiative effects. *J. Geophys. Res.*, **109**, D23203, doi:10.1029/2004JD004827.
- Ward, D. E., and Coauthors, 1992: Smoke and fire characteristics for cerrado and deforestation burns in Brazil: Base-B experiment. *J. Geophys. Res.*, **97**, 14 601–14 619.
- , W. M. Hao, R. A. Susott, R. E. Babbitt, R. W. Shea, Y. J. Kaufman, and C. O. Justice, 1996: Effect of fuel composition on combustion efficiency and emission factors for African savanna ecosystems. *J. Geophys. Res.*, **101**, 27 361–27 371.
- Weaver, C., P. Ginoux, N. Hsu, M.-D. Chou, and J. Joiner, 2002: Radiative forcing of Saharan dust: GOCART model simulations compared with ERBE data. *J. Atmos. Sci.*, **59**, 736–747.
- Weaver, C. J., J. Joiner, and P. Ginoux, 2003: Mineral aerosol contamination of TOVS temperature and moisture retrievals. *J. Geophys. Res.*, **108**, 4246, doi:10.1029/2002JD002571.